



Contents lists available at SciVerse ScienceDirect

Journal of Asian Earth Sciences

journal homepage: www.elsevier.com/locate/jseas

Kinematics of the crust around the Ama Drime Massif (southern Tibet) – Constraints from paleomagnetic results

C. Crouzet^{a,*}, E. Appel^b, R. El Bay^b, L. Ding^c, I. Dunkl^d, C. Montomoli^e, R. Carosi^f, Q.H. Zhang^{c,g}, B. Wauschkuhn^h^a Institut des Sciences de la Terre, Université de Savoie, CNRS, 73376 Le Bourget du Lac, France^b Fachbereich Geowissenschaften, Universität Tübingen, Sigwartstrasse 10, 72076 Tübingen, Germany^c Institute of Tibetan Plateau Research, Chinese Academy of Sciences, No. 18, Shuangqing Rd., Beijing 100085, PR China^d Geowissenschaftliches Zentrum der Universität Göttingen, Goldschmidtstr. 3, 37077 Göttingen, Germany^e Dipartimento Scienze della Terra, via S. Maria 53, 56126 Pisa, Italy^f Dipartimento Scienze della Terra, via Valperga Caluso 35, 10125 Torino, Italy^g Fachbereich Geowissenschaften, Universität Bremen, Postfach 330 440, 28334, Bremen, Germany^h Institut für Geowissenschaften, Technische Universität Bergakademie Freiberg, Bernhard-von-Cottastr. 2, 09596 Freiberg/Sachsen, Germany

ARTICLE INFO

Article history:

Received 3 October 2011

Received in revised form 12 June 2012

Accepted 13 June 2012

Available online 23 June 2012

Keywords:

Paleomagnetism

Himalaya

Pyrrhotite

Rotation

Tilting

Secondary magnetization

Ama Drime

ABSTRACT

Secondary magnetic remanences are used to study late-orogenic rotation and tilting on a E–W transect in southern Tibet at $\sim 28.5^\circ\text{N}$. Sampling was performed on both sides of the Ama Drime Massif (ADM). Remanent magnetization resides in pyrrhotite formed during metamorphism and is related to the last cooling event through 325°C (Curie temperature of pyrrhotite). The existence of antipodal pTRMs demonstrates that the ChRM is of thermoremanent origin and was acquired during cooling of the Tethyan metasediments. Penetrative deformation was still going on in Rongbuk area until ca 250°C , whereas it was already completed in Dinggye area. Significant departures from the expected field direction during the age of remanence acquisition cannot be interpreted by consistent vertical axis rotation of blocks. Antagonist deviations on both sides of the ADM are explained as tiltings around an horizontal axis striking $\sim \text{N}20^\circ$. These tiltings are estimated to be younger than 13–12 Ma and they are related to the ADM exhumation initiated since 33 Ma.

© 2012 Elsevier Ltd. All rights reserved.

1. Introduction

How continental crust responds to plate collision is one of the major still open questions in geodynamics. The India–Asia collision and ongoing convergence resulted in the building of the Himalayan orogen and the development of the Tibetan Plateau (Hodges, 2000). The mechanisms and time required to build these spectacular geotectonic features seem to be still unsolved (see discussion in Gloaguen and Ratschbacher, 2011). In this context, motions of crustal blocks like translation, rotation or tilting, are important parameters that paleomagnetic studies may evidence quantitatively.

In the western part of the Himalaya, oroclinal bending is well reflected by palaeomagnetic data (Schill et al., 2001). In contrast, data from the central part (Schill et al., 2004) and recent results from the eastern part (Antolín et al., 2010) indicate palaeomagnetic rotations, which are not compatible with an oroclinal bending model. It can be hypothesised that eastward extrusion of the Tibetan Plateau left its fingerprint in a long-term deformation of the

Himalayan region forming a large-scale shear zone with strong clockwise block rotations and sinistral strike-slip faults between individual blocks (Schill et al., 2004).

In the Tethyan Himalaya, secondary pyrrhotite remanences have been widely used to provide significant results all along the Himalayan range from Zanskar in the West (Appel et al., 1995) to southeastern Tibet (Antolín et al., 2010). In our present study we have conducted sampling along an E–W transect from 86.5 to 88°E , close to the South Tibetan Detachment System (STDS), in an area which represents a gap of paleomagnetic data in between previously published results. In this region the Ama Drime Massif (ADM) is an outstanding tectonic crustal feature which has been described in recent works of Leloup et al. (2010) and Kali et al. (2010).

2. Geological setting

The studied area is situated in the Tethyan Himalaya (TH), comprising the Tibetan Sedimentary Series (TSS), which is developed all along the Himalayan arc and represents the deformed remnant of the passive northern margin of the Indian subcontinent (Garzan-

* Corresponding author. Tel.: +33 4 79 75 94 55.

E-mail address: christian.crouzet@univ-savoie.fr (C. Crouzet).

ti, 1999). The Indus–Yarlung Suture Zone (IYSZ) in the north and the South Tibetan Detachment System (STDS) in the south tectonically bound the TH zone (Fig. 1). The sedimentary pile has a thickness of ~ 6–7 km and is made up of a fairly complete and well-preserved Cambro-Ordovician to Eocene succession (Bassoulet et al., 1980; Brookfield, 1993; Garzanti, 1999). The tectonic evolution of the TH is well constrained in central Nepal (Godin, 2003; Kellett and Godin, 2009; Larson et al., 2010) and in some well accessible places in southern Tibet (Ratschbacher et al., 1994; Zhang and Guo, 2007) with several folding and faulting phases of opposite vergencies (Carosi et al., 2002, 2007; Montomoli et al. 2008; Antolín et al., 2011). Close to the STDS, the TSS has undergone intense deformation and Barrovian type metamorphism with P–T conditions up to 3–6 kbar and 600–650 °C (Vannay and Hodges, 1996; Jessup et al., 2008; Dunkl et al., 2011). Elsewhere, mainly diagenetic conditions to low-grade metamorphism were evidenced (Fuchs, 1967; Crouzet et al., 2007).

The present study focuses on the TH located around the Ama Drime Massif (ADM). It is the transition between the High Himalayan range and the TH of southern Tibet and is an active N–S horst that may offset the STDS (Zhang and Guo, 2007; Leloup et al., 2010). The ADM contains the only eclogite found in the central Himalayas (Lombardo and Rolfo, 2000; Groppo et al., 2007) that implies exhumation of deep-seated rocks. The deepest rocks from the ADM were buried up to 14–16 kbar (ca ~50–60 km depth) during Eohimalayan metamorphism at ~33 Ma (Liu et al., 2007; Kali et al., 2010).

The ADM exhumation can be related to the simultaneous activity of the Main Central Thrust (MCT) and the STDS, and to E–W

extension latter on. A change in the tectonic behavior initiated N–S normal faults prior to 11 Ma. The resulting E–W extension have accounted for a total of about 22 km of exhumation (Kali et al., 2010; Langille et al., 2010). According to geomorphologic features visible in the field, the normal faults bounding the Ama Drime Massif are probably still active. Triangular facets and offsets of fluvial terraces or tills are visible in the landscape and have been reported by several authors (Armijo et al., 1986; Zhang and Guo, 2007; Kali et al., 2010).

3. Sampling and laboratory procedures

Field work in southern Tibet has been carried out along an E–W section between 86°45' and 88°E (Fig. 2) on both sides of the Ama Drime Massif during two campaigns. A total of 43 sites from low grade Ordovician to mid-Triassic metacarbonates and slates were sampled (23 sites from the western part: Pazhug village area, Khar-ta and Rongbuk valleys and 20 sites from the Dinggye area east of the Ama Drime Massif).

A portable gasoline-powered rock drill was used for taking cores of 2.5 cm in diameter, which were oriented in situ with a magnetic compass. Generally, 10 cores (6–10 cm in length) were obtained from each site and cut into standard specimens of 2.2–2.4 cm length. The following instruments were used: a Kappabridge KLY-2 (Agico) for measuring anisotropy of susceptibility (AMS) and for monitoring bulk susceptibility after each heating step; a 755R SQUID magnetometer (2G Enterprises) with a noise level of ~0.005 mA m⁻¹ (for 10 cm³ samples) for remanence mea-

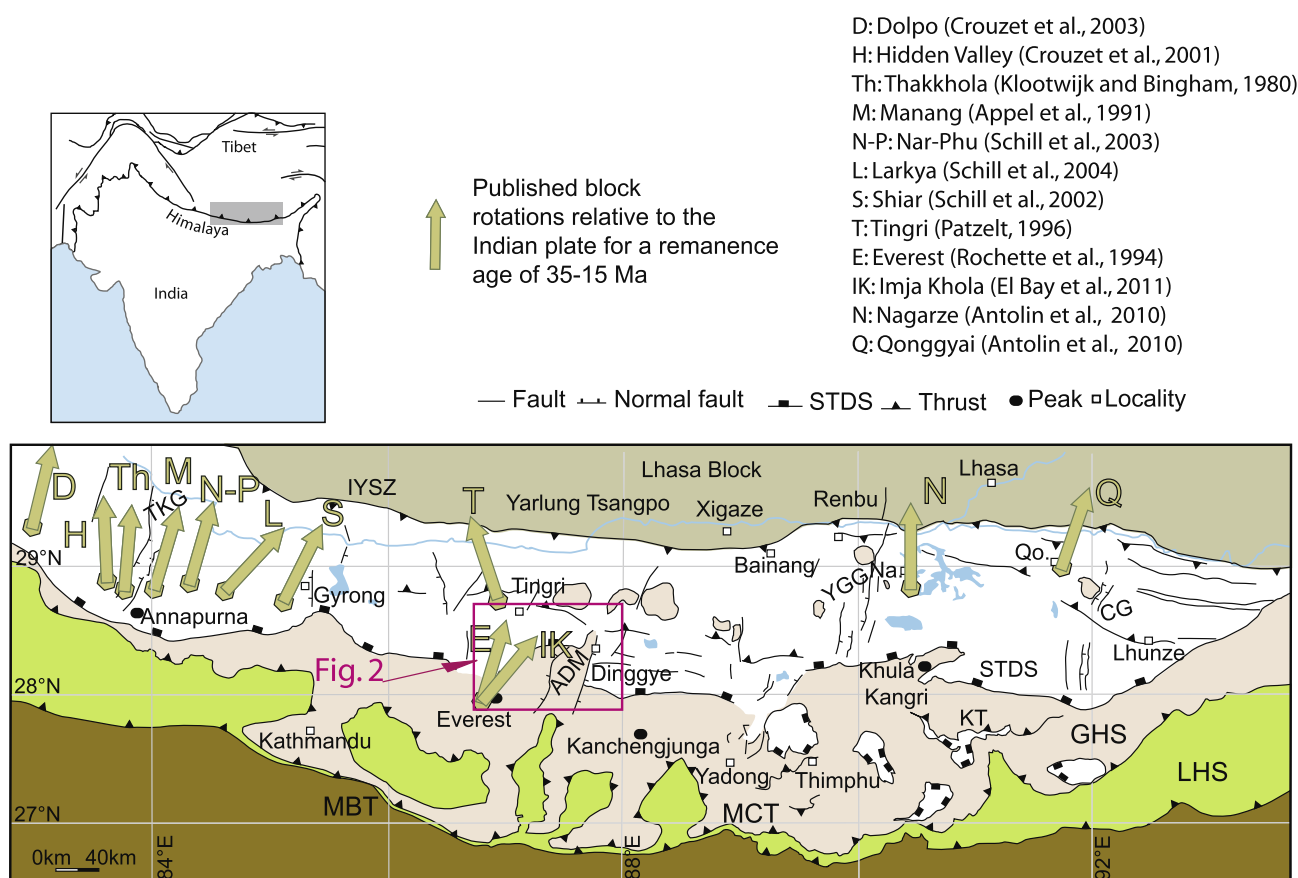


Fig. 1. Geological map of the central and eastern Himalaya (after Antolín et al., 2010; modified) with published paleomagnetic rotations (remanence ages between 35 and 15 Ma). TKG, Thakkhola Graben; IYSZ, Indus Yarlung suture zone; ADM, Ama Drime Massif; YGG, Yadong–Gulu Graben; Na, Nagarze; Qo, Qonggyai; CG, Cona Graben; STDS, South Tibetan Detachment System; KT, Kakhtang thrust; GHS, Greater Himalayan sequence; MCT, Main Central Thrust; LHS, Lesser Himalayan sequence; MBT, Main Boundary Thrust. Location of Fig. 2 is indicated. (see above-mentioned references for further information.)

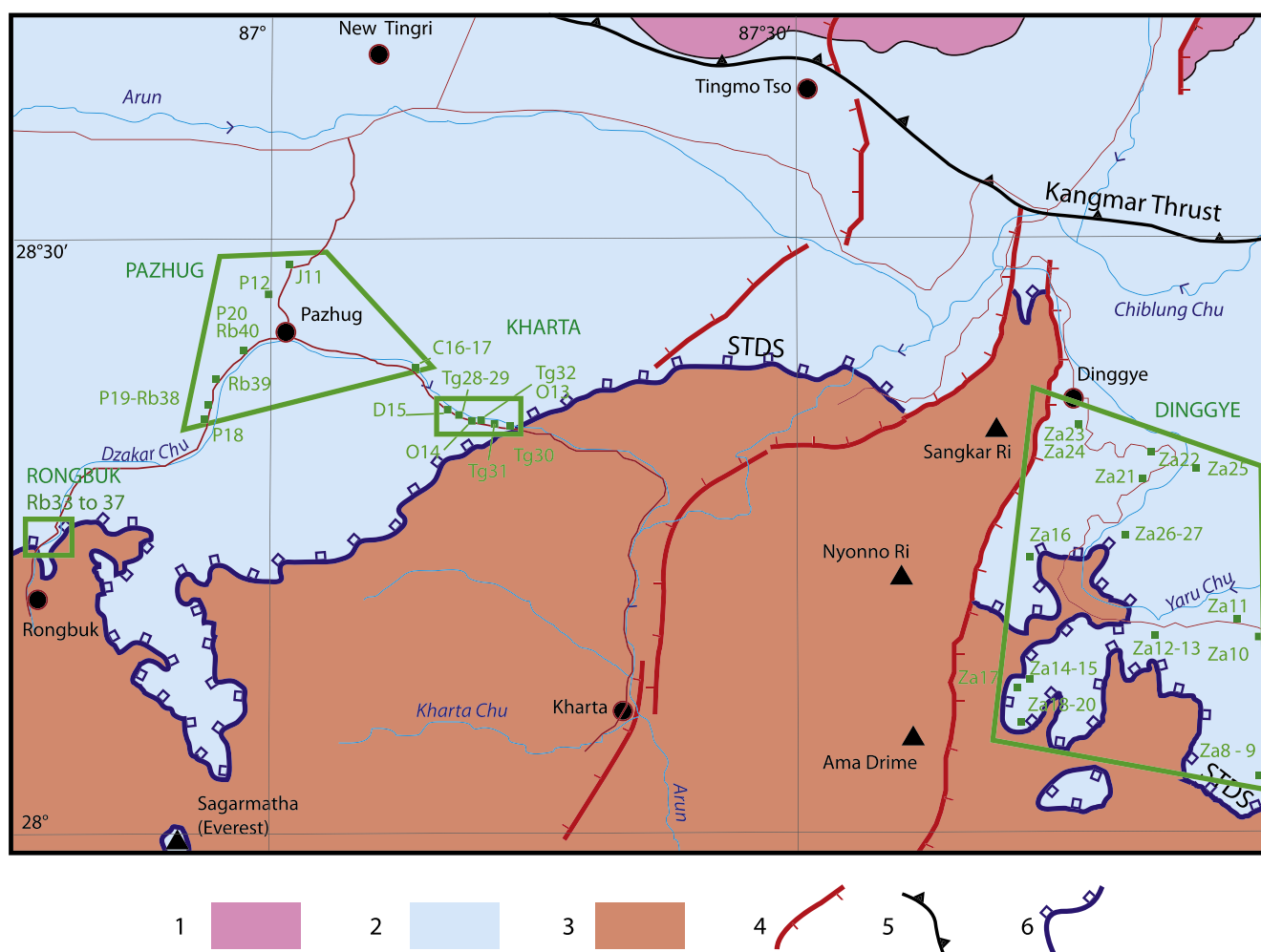


Fig. 2. Structural map (after Kali et al., 2010; modified) with sampling areas and site locations (green boxes and squares). 1: North Himalayan granitoids. 2: Tethyan Sedimentary Series. 3: Undifferentiated Himalayan Crystalline Series. 4: Normal faults bounding the ADM. 5: Thrust. 6: Detachment.

measurements; a static tri-axial demagnetizer (2G Enterprises) of 150 mT maximum field for alternating field demagnetization (AFD); a MMTD18 or MMTD60 furnace (Magnetic Measurements) for progressive thermal demagnetization (ThD); a MMPM9 pulse magnetizer (Magnetic Measurements) with 2.5 T maximum field to impart isothermal remanent magnetization (IRM), and a fluxgate spinner magnetometer (Molspin) with a noise level $\sim 0.2 \text{ mA m}^{-1}$ (for 10 cm^3 samples) to measure IRM. All these measurements were carried out at the palaeomagnetic laboratory of Tübingen University. Thermomagnetic measurements were performed on selected samples with a Quantum Design XL7 MPMS (noise level $\sim 10^{-11} \text{ A m}^2$ at Bremen University. Room temperature (RT) saturation isothermal remanence magnetization (SIRM^{RT}) runs were done on selected samples using a DC field – applied at RT – with a magnitude of 5 T; cycling from 300 to 5 K (field cooling) and back to room temperature (field warming) in zero-field was monitored in 2.5 K increments.

The data set obtained by demagnetization was analysed using the PALMAG software, developed in-house at the University of Munich. This software comprises standard tools for processing, displaying and analysing palaeomagnetic data, including principal component analysis (PCA, Kirschvink, 1980) and remagnetization circle analysis following the algorithm of McFadden and McElhinny (1988). The fold test was performed using the PMGSC software v.4.2 (Enkin, 2004).

4. Magnetic mineralogy and remanence directions

The 10 sites collected from very low grade Carboniferous to Triassic carbonates close to Pazhug village (Fig. 2) show the occurrence of mainly hematite and / or magnetite with partly small amounts of pyrrhotite. Overlapping of unblocking temperature spectra for pyrrhotite and iron oxides is evidenced from SIRM acquisition and subsequent thermal demagnetization (Fig. 3). Therefore, the PCA analysis became sometimes ambiguous and the interpretation in terms of block rotation hazardous. In the following, we will focus only on those sites containing predominantly pyrrhotite as the carrier of remanence.

For sites sampled close to the STDS, mainly Ordovician, IRM acquisition and subsequent thermal demagnetization of SIRM evidence the occurrence of mainly pyrrhotite (Fig. 3A and B). Residual magnetization after thermal treatment is probably due to a small contribution of hematite and/or magnetite. During AF treatment up to 140 mT, usually only 20–50% of the NRM was removed (Fig. 3C), attesting the occurrence of a relatively high coercivity magnetic mineral. Low temperature thermomagnetic measurements evidenced a clear transition at $\sim 32 \text{ K}$ (Fig. 3D), confirming the occurrence of monoclinic pyrrhotite (Besnus, 1966; Rochette et al., 1990, 2011). NRM thermal demagnetization demonstrates the dominance of a low temperature component, removed at maximum $\sim 320\text{--}350 \text{ }^\circ\text{C}$ (Fig. 4), which can be related to pyrrhotite.

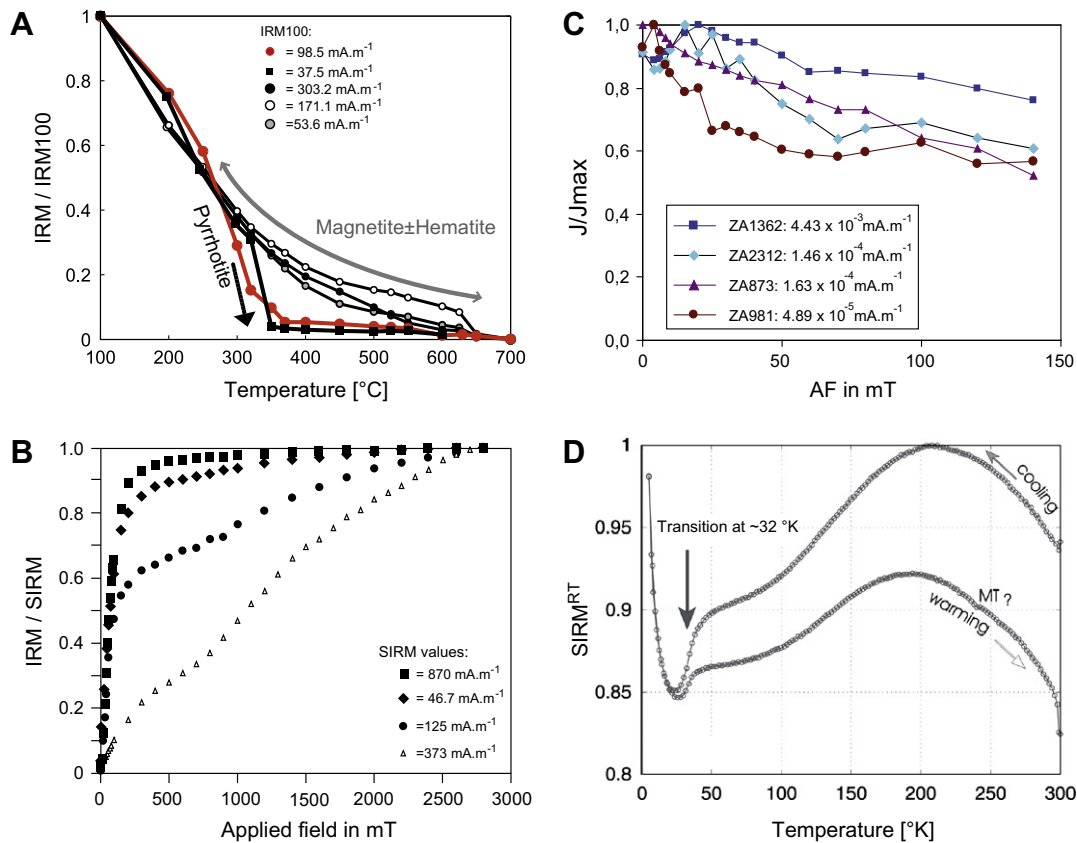


Fig. 3. Magnetic mineralogy. A: IRM acquisition curves for samples showing mainly pyrrhotite (full symbols) and for comparison sample containing mainly hematite (open triangle). B: Examples of SIRM thermal demagnetization showing overlapping of unblocking spectra for samples from Carboniferous to Triassic (open symbols) in comparison to Ordovician samples with mainly pyrrhotite (full symbols) and a small content of magnetite and possibly also hematite. C: Examples of intensity decay during AF demagnetization of NRM. D: Field cooling (300–5 °K) and warming (5–300 °K) of 5 T room temperature (RT) SIRM for samples from Kharta and Dinggye areas. Evidence of monoclinic pyrrhotite is given by the Besnus transition at ~32 °K (Besnus, 1966 and Rochette et al., 2011). The large decrease/increase in remanence between 20 and 5 K is most likely related to paramagnetic particles.

For Dinggye area, PCA analysis reveals stable and well grouped ChRM directions at site scale with $k > 10$ (Fig. 5 and Table 1). In a given site, all the samples have usually the same polarity. A better grouping of the site mean directions before tectonic correction is observed ($k_{insitu}/k_{bed} = 2.6$). The optimum degree of untilting (Watson and Enkin, 1993) is reached at $12.7 \pm 9.4^\circ$, indicating remagnetization after or at the end of the deformation (Fig. 6). The distribution of site mean directions, in geographic coordinates indicates a small circle distribution (Fig. 5). Assuming a horizontal axis for the small circle distribution, the best fit direction of the cone is $\sim 350^\circ$ with an opening angle of 32° and this small circle contains the regional site mean direction obtained by Fisher statistics. The dispersion along a small circle can be interpreted as the effect of local tilting due to the Xainza – Dinggye normal fault zone system.

In the western areas (Pazhug, Kharta and Rongbuk areas) 13 out of in total 23 sites reveal a magnetization carried only by pyrrhotite. These 13 sites are located close to the STDS and the origin of pyrrhotite magnetization is probably due to a higher metamorphic grade.

In Kharta area, a very similar demagnetization behavior was observed with a component removed usually in between 250 and 340 °C range corresponding to pyrrhotite (Fig. 4). This component shows a reverse polarity in 5 out of 8 sites (Table 2). The regional in situ mean direction is $D/I = 20.6^\circ/37.5^\circ$ ($k = 51.9$, $\alpha_{95} = 6.9^\circ$, $N = 8$). The fold test is negative (with $k_{insitu}/k_{bed} = 8.2$, indicating a post-folding age for the NRM (Figs. 6 and 7). Also, the optimum degree of untilting is $3.7 \pm 11.9^\circ$. In site Tg31, it was possible to extract two more or less antiparallel components. The LT one (300–

310 °C) yields a reverse polarity ($D/I = 172.1^\circ/-42.3^\circ$, $k = 18.6$, $\alpha_{95} = 16.3^\circ$, 4 specimens), while the HT one (310–340 °C) represents a normal polarity ($D/I = 32.1^\circ/38.2^\circ$, $k = 14.3$, $\alpha_{95} = 15.1^\circ$, 7 specimens). These two directions are statistically different. As the HT one is more similar to the expected field direction during the age of remanence acquisition (see discussion below), it may be explained by ongoing deformation (rotation and/or tilting) during cooling.

In the Rongbuk area, several components have been evidenced over the pyrrhotite unblocking temperature range (Fig. 8). A HT component ($>310^\circ\text{C}$) is north directed with inclination close to zero and is obviously of normal polarity (N1). A LT component (280–310 °C) is south directed (reverse polarity) with very shallow inclination (R1). Between 250–280 °C and 150–250 °C two more components of normal (N2) and reverse (R2) polarities were extracted (Table 3). In site Rb 37 even a third normal component (N3) occurred at very low temperature. In few samples it was also possible to evidence a HT reverse component (see sample Rb35-1a on Fig. 8). The record of successively normal and reverse component versus temperature confirms the thermal origin of the NRM as evidenced in several other places of the Alps (Ménard and Rochette, 1992; Crouzet et al., 1997, 2001a) and in the Himalaya (Crouzet et al., 2001b) and interpreted as remanences acquired during exhumation. In the present study, due to field constraints, it was not possible to sample along a profile perpendicular to the paleo-isotherms. The fold test is indeterminate for the N1 component and possibly negative for the R2 component (Fig. 9). We must be aware that the statistic parameters do not allow to interpret the data from the Rongbuk area unambiguously. While similar bedding

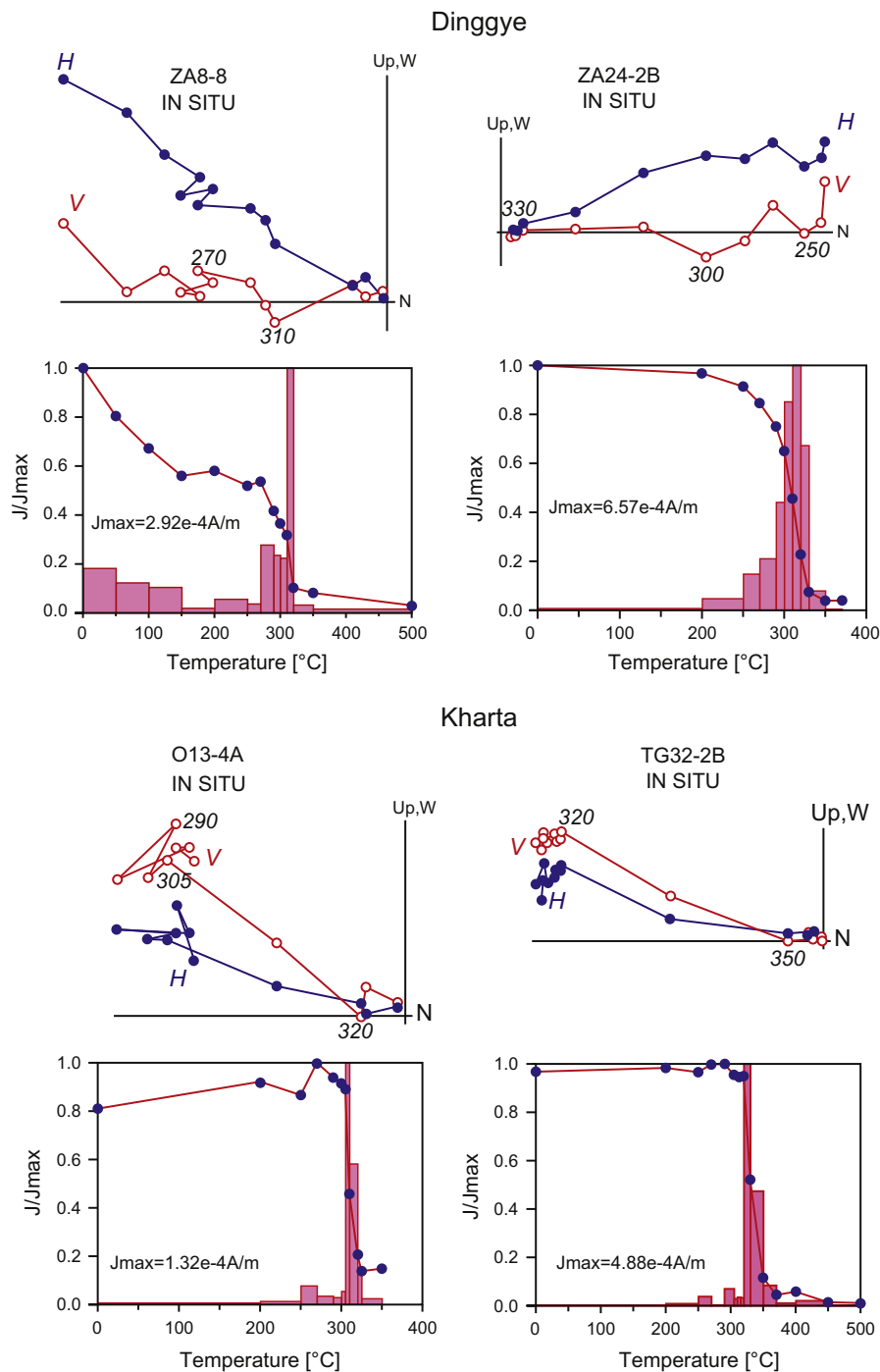


Fig. 4. Examples of stepwise thermal demagnetization of NRM (orthogonal vector projections and intensity curves) for samples from (A) Kharta area and (B) Dinggye area. Solid (open) symbols are horizontal (vertical) plane projections.

attitudes disable the efficiency of the fold test, the significant (within α_{95}) deviation from the expected direction during remanence acquisition (see complete discussion in the next paragraph) indicates that the HT component (N1) may be pre-folding while lower temperature R2 component may post-date folding (Fig. 10).

5. Discussion

5.1. Nature and age of remanence

Several investigations have demonstrated that monoclinic pyrrhotite can record stable paleomagnetic signals in low-grade meta-

morphic rocks like marly limestones and slates (e.g. Carpenter, 1974; Rochette, 1987; Appel et al., 1991; Ménard and Rochette, 1992; Crouzet et al., 1996, 2001a, 2001b; Gillett, 2003; Schill et al., 2004; Antolín et al., 2010). Also, the origin of pyrrhotite in the low-grade metamorphic rocks and the nature of its remanence has been discussed in several papers (e.g. Crouzet et al., 2003; Wehland et al., 2005; Kim et al., 2009 and reference therein).

The age of the magnetization in Rongbuk area probably coincides with the deformation phase associated to the motion along the STDS. According to the studies of Godin et al. (2006) and Kellett and Godin (2009) in central Nepal, an age of 22–18 Ma can be proposed. In the Ama Drime area, the motion along the STDS has been

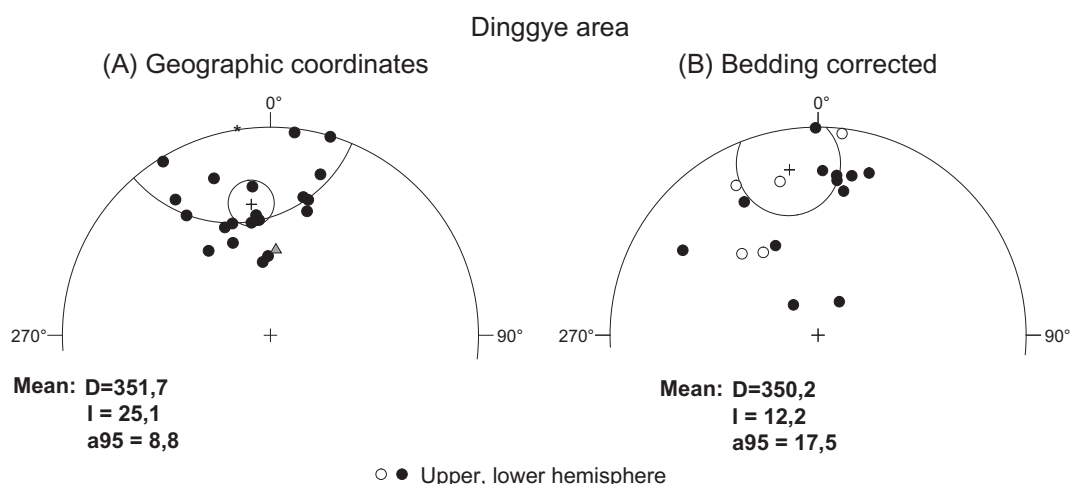


Fig. 5. Stereographic projection of the pyrrhotite site mean directions for Dinggye area. The overall mean direction obtained by Fisher statistics is indicated. Open (solid) circles are projected in the upper (lower) hemisphere. (A) In situ (geographic coordinates), (B) Bedding corrected; all site mean directions plotted as normal polarity. The present-day dipole field direction is indicated by a triangle in (A).

Table 1
Site mean directions and regional mean direction for Dinggye area. Dec: declination; Inc: inclination; *k*: Fisher's (1953) concentration parameter; α_{95} : 95% confidence angle; N: number of useful samples; NO: number of collected samples. Site location (latitude and longitude) is indicated. All samples have the same polarity in a site.

Site	Lat (N)	Long (E)	N/NO	Geographic				Bedding			
				Dec	Inc	<i>k</i>	α_{95}	Dec.	Inc.	<i>k</i>	α_{95}
za8	28.06301	87.98063	6/9	13.4	21.4	31.8	10.1	17.5	11.5	31.8	10.1
za9	28.0626	87.9803	5/7	16.5	26.3	41.5	9.7	No bedding data			
za10	28.1619	87.9738	8/8	337.9	38.8	19.4	12.9				
za11	28.1714	87.9470	5/6	353.2	29.7	14.4	16.5				
za12	28.1751	87.8744	4/8	161.2	-30.9	15.1	24.4	166.1	15.5	15.1	24.4
za13	28.1752	87.8692	6/6	178.3	-48.3	57.2	7.6	186.7	-14.6	57.2	7.6
za14	28.1375	87.7107	3/6	195.6	-21.9	19.7	18.2	187.0	-16.3	19.7	18.2
za15	28.1384	87.7096	5/6	17.3	12	12.9	22.1	12.0	13.9	12.9	22.1
za16	28.2400	87.7398	5/7	323.8	36.6	130.6	5.5	320.8	68.8	130.6	5.5
za17	28.0756	87.4258	4/6	354.4	31.8	15	18.1	334.6	39.1	15.0	18.1
za18	28.1060	87.7011	4/5	337.1	31.3	17.4	16.8	331.0	17.6	17.4	16.8
za19	28.1088	87.6999	4/5	6.8	1.1	15.3	17.9	6.8	-1.4	15.3	17.9
za20	28.1091	87.7018	8/10	328.3	1.1	24.2	10.1	331.3	-11.3	24.2	10.1
za21	28.3138	87.8585	4/6	354.0	51.0	11.7	20.4	10.1	19.8	11.7	20.4
za22	28.3243	87.8504	5/11	325.0	13.0	11.0	18.9	302.1	15.0	11.0	18.9
za23	28.3298	87.7770	5/7	340.2	12.6	10.5	19.3	326.5	-39.0	10.5	19.3
za24	28.3343	87.7791	7/8	16.8	0.2	13.9	14.2	32.6	68.4	13.9	14.2
za25	28.3090	87.8967	4/6	325.0	19.8	17.8	22.4	316.9	-33.7	17.8	22.4
za26	28.2468	87.8167	7/7	353.1	18.5	18.8	12.2	359.3	0.2	18.8	12.2
za27	28.2446	87.8200	8/9	350.4	32.5	81.1	5.5	1.6	13.3	81.1	5.5
Mean	28.1981	87.7964	20	351.7	25.1	13.1	9.4	350.2	12.2	5.1	17.5

Means are calculated with all sites as normal polarity.

dated between 19 and 13 Ma (see discussion in Kali et al., 2010) Also this deformation phase is usually characterized by SC fabric and microfolds (Godin, 2003; Crouzet et al., 2007; Leloup et al., 2009, 2010). Internal deformation occurring during cooling can explain the magnetic behavior observed in the Rongbuk area. Therefore, for determining block rotation, we should use only the lower temperature component recorded. This component is likely post-folding and close to the expected Earth magnetic dipole field direction at 20 Ma.

In Dinggye area, 3 sites over a total of 20, present a reverse polarity (Table 1) indicating a thermoremanent origin for the magnetization (i.e. temperature during metamorphism above the Curie temperature of pyrrhotite $T^{\circ}\text{C} \sim 320^{\circ}\text{C}$). Paleotemperature data for Ordovician limestone sampled in the same area, obtained through calcite-dolomite geothermometers supported by microstructural analyses (i.e. deformation mechanisms and syntectonic twinning

in calcite) span from 320–360 °C (Montomoli et al., 2009) are in agreement with the above results. In Kharta area, 5 sites over a total of 8 have a reverse polarity (Table 2). Also the occurrence of antipodal components in site Tg31 is a strong indicator for a thermoremanent origin of the magnetization. As it requires growth of pyrrhotite crystals of different size at different times, a chemical or thermochemical origin is very unlikely (Crouzet et al., 2001b). Normal and reverse polarities observed at the regional scale and antipodal behavior within single specimens confirm that the observed magnetic remanences have been acquired throughout a sufficiently long time span to allow averaging on palaeosecular variation.

One may question the occurrence of 4 well defined components of opposite polarities in the Rongbuk samples. In fact it has been clearly demonstrated by comparing NRM and laboratory TRM (pseudo-Thellier experiments) that more reversals can be retrieved

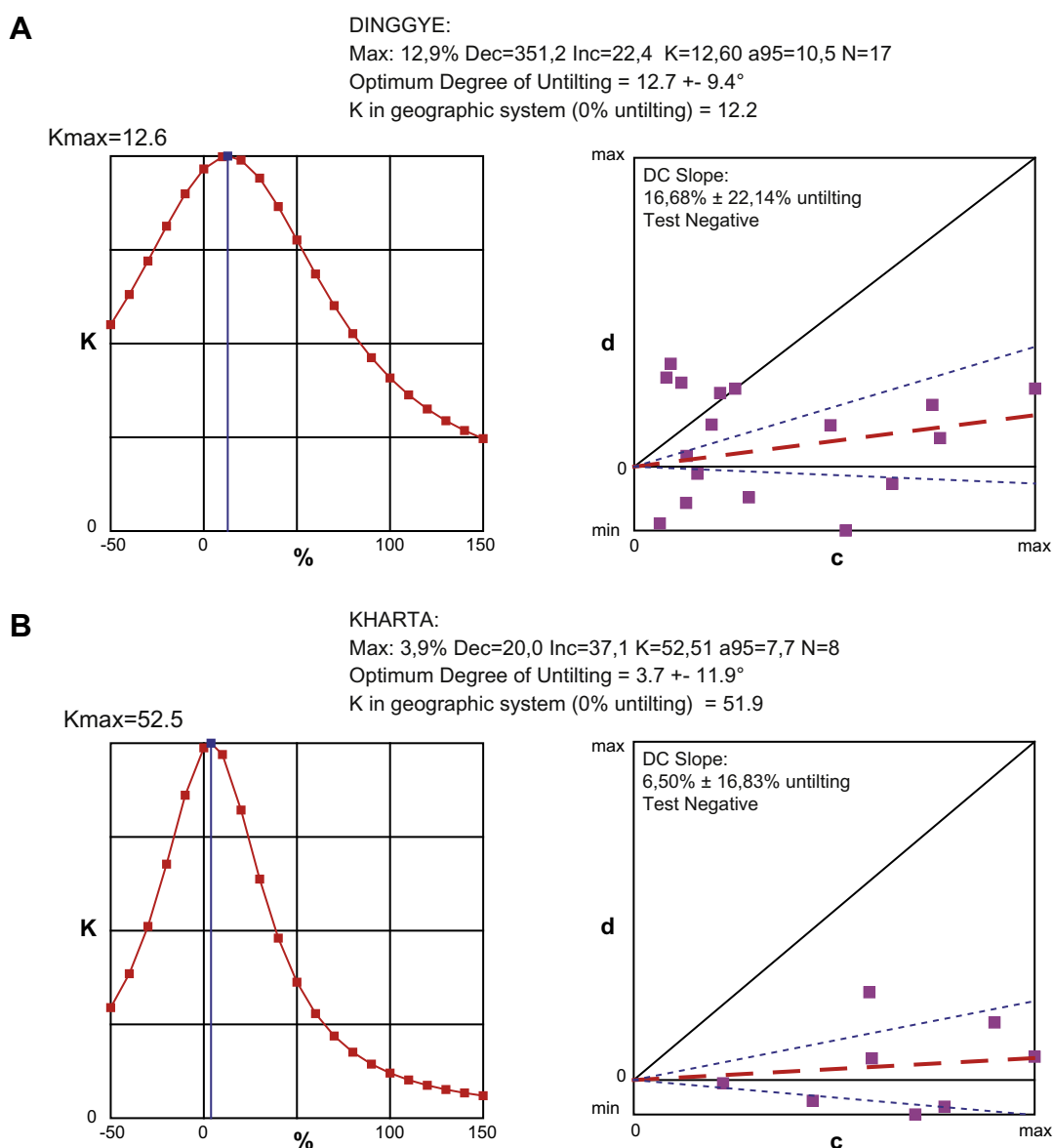


Fig. 6. Fold tests for (A): Dinggye and (B): Kharta areas. Left side: Classical k ratio test (calculated after Enkin, 2004) showing statistical results from stepwise unfolding. The optimum degree of untilting (ODU) according to Watson and Enkin (1993) is indicated (accuracy of bedding attitude was arbitrarily taken equal to 3°). Right side: DC tilt test results showing d versus c, where c is the angle between the geographic mean direction and the tilt-corrected site-mean direction that is back rotated by the angular relationship between the two directions and d is a projection of the arc between geographic site-mean directions and the geographic mean of means direction onto the arc used to calculate the c value (Enkin, 2003). Optimal clustering is not significantly different than 0%, indicating a negative tilt test result. Dashed line indicates mean untilting percent; dotted lines indicate error bars.

Table 2

Site mean directions and regional mean direction for Kharta area. All samples have the same polarity in a site. T° range: the temperature range over which the component was extracted, for other abbreviations see Table 1.

Site	Lat (N)	Long (E)	T° range	N/N ₀	Geographic				Bedding			
					Dec.	Inc.	k	α ₉₅	Dec.	Inc.	k	α ₉₅
Tg30	28.3501	87.2003	290–335	5/5	32.3	49.9	24.1	12.8	22.6	12.6	24.1	12.8
Tg31	28.3513	87.1913	310–340	6/7	32.1	38.2	14.3	15.1	21.5	1.8	14.3	15.1
Tg32	28.3517	87.1860	250–350	6/6	207.2	–30.8	34.6	9.7	196.9	–0.8	34.6	9.7
O13	28.3525	87.1856	270–330	9/10	212.6	–34.5	109.7	4.5	200.7	–15.0	109.7	4.5
O14	28.3537	87.1825	300–325	5/7	193.5	–34.0	15.0	16.2	189.8	12.9	15.0	16.2
Tg29	28.3557	87.1807	200–350	6/6	1.3	42.6	15.9	14.4	329.4	51.0	15.9	14.4
Tg28	28.3565	87.1798	290–350	4/6	193.9	–30.8	11.4	20.7	167.8	–52.3	11.4	20.7
D15	28.3595	87.1730	290–320	8/10	193.0	–35.5	26.2	9.7	157.7	–59.4	26.2	9.7
Mean	28.3539	87.1849		8	20.6	37.5	51.9	6.9	8.1	23.3	6.3	19.7

Means are calculated with all sites as normal polarity.

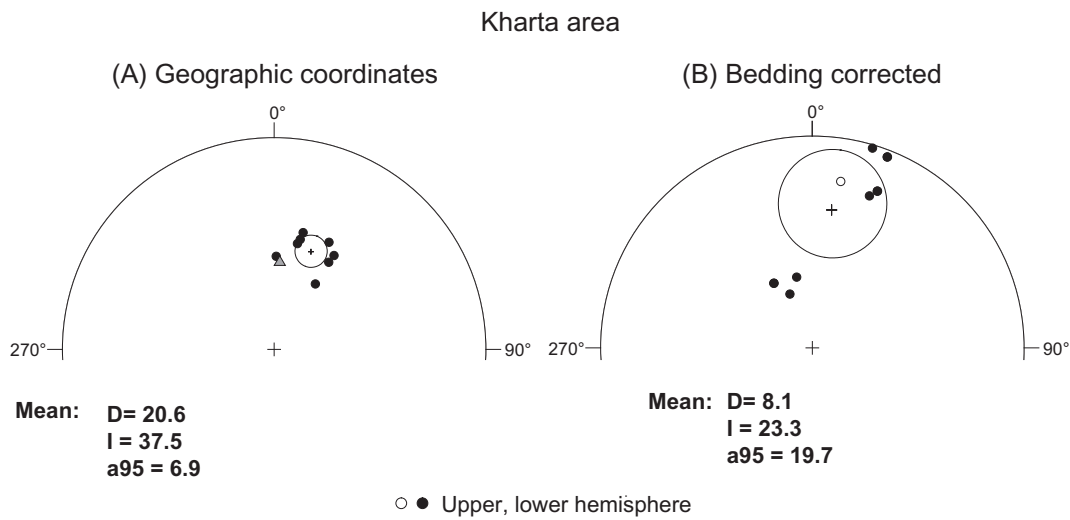


Fig. 7. Stereographic projection of the pyrrhotite site mean directions for Kharta area. The overall mean direction obtained by Fisher statistics is indicated. Open (solid) circles are projected in the upper (lower) hemisphere. (A) In situ (geographic coordinates with all site mean directions plotted as normal polarity), (B) Bedding corrected. The present-day dipole field direction is indicated by a triangle in (A).

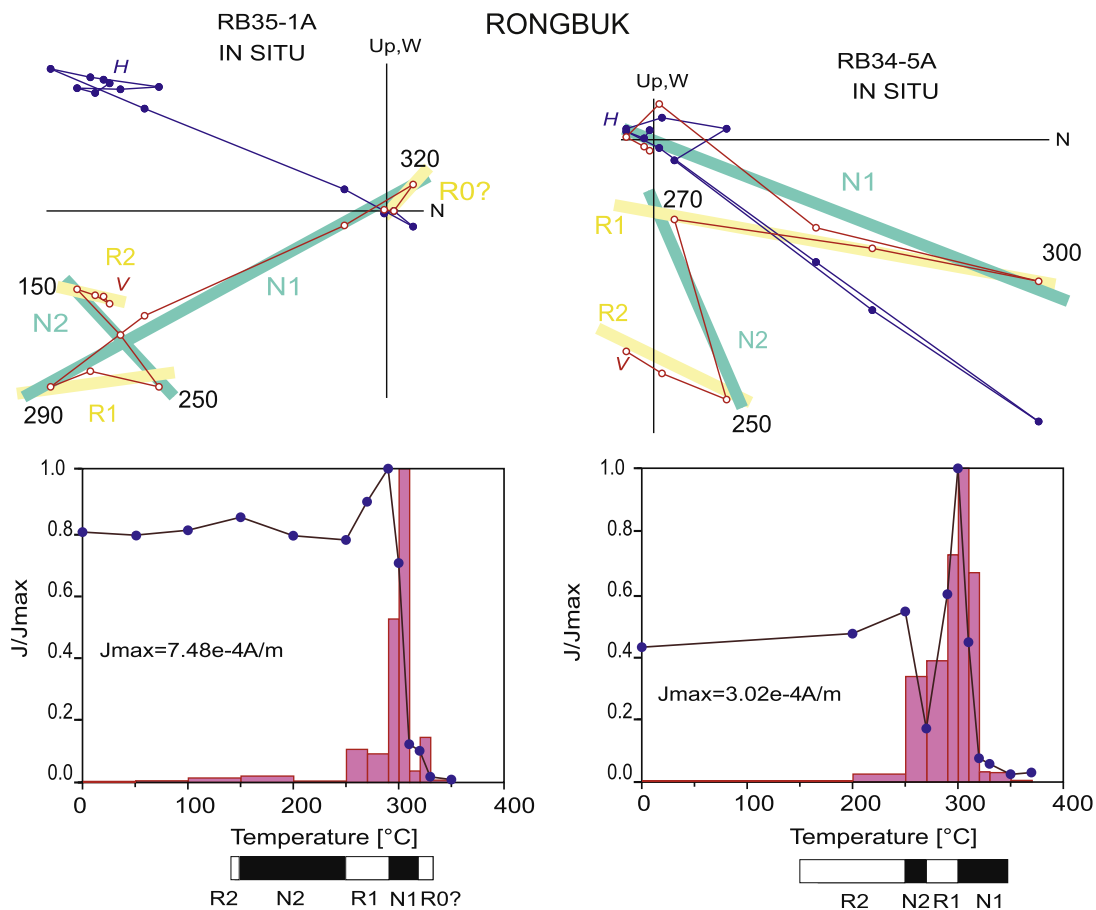


Fig. 8. Examples of thermal demagnetization of NRM (orthogonal vector projections and intensity curves) for samples from Rongbuk area, showing several antipodal components (N1, R1, N2 and R2). Solid (open) symbols are horizontal (vertical) plane projections.

(Crouzet et al., 2001a). This filtering effect depends of the cooling rate, the pyrrhotite grain size distribution and the frequency of reversals during cooling.

In order to evidence possible rotations of the studied area, determination of the age of the magnetization is crucial. Inclina-

tion matching is very uncertain because several complications may have occurred since the time of magnetization (rotation around an horizontal axis, N–S crustal shortening). In the studied area, no geochronological data are available in the TSS. The age of the peak temperature in the Ama Drime orthogneiss is 20–

Table 3

Site mean directions and regional mean direction for the different antipodal components of Rongbuk area. See Table 1 for legend.

Site	Lat (N)	Long (E)	T° range	Geographic coordinates					Bedding corrected				
				N/N ₀	Dec.	Inc.	k	α ₉₅	N/N ₀	Dec.	Inc.	k	α ₉₅
<i>Normal 1</i>													
Rb33	28.27881	86.81017	>T°c?	–						–			
Rb34	28.27697	86.72598	300–Tc	3/5	23.0	10.4	27.7	15.4	3/5	20.4	29.1	27.7	15.4
Rb35	28.28358	86.80595	310–Tc	3/7	31.2	–22.4	7.8	28.9	3/7	30.0	–3.1	7.8	28.9
Rb36	28.28107	86.80388	310–Tc	6/7	8.0	–1.4	12.9	15.9	6/7	9.31	26.2	23.2	11.9
Rb37	28.28251	86.81231	315–Tc	3/7	13.4	11.8	9.2	32.7	3/7	No structural data			
		Mean	310–Tc	4	18.6	–0.2	19.2	21.5	3	20.3	17.7	16.1	31.8
<i>Reverse 1</i>													
Rb33	28.27881	86.81017	270–Tc	5/6	211.5	5.9	14.8	16.3	5/6	211.2	–12.0	27.4	12.0
Rb34	28.27697	86.72598	290–300	2/5	315.8	35.7	11.9	28.7	2/5	305.5	39.2	26.0	19.4
Rb35	28.28358	86.80595	290–310	7/7	205.2	19.4	34.0	9.1	7/7	204.6	–0.3	34.0	9.1
Rb36	28.28107	86.80388	280–310	7/7	195.1	1.1	46.2	7.8	7/7	190.4	–26.3	74.2	6.1
Rb37	28.28251	86.81231	290–315	3/7	195.7	–39.3	20.3	17.9	3/7	No structural data			
		Mean	280–310	5	214.7	6.7	2.6	59.6	4	218.2	–0.5	2.4	76.0
			4 (–Rb 34)		202.2	–2.8	9.6	31.2	3 (–Rb 34)	202.4	–13.0	24.3	25.6
<i>Normal 2</i>													
Rb33	28.27881	86.81017	250–270	3/6	12.0	57.4	125.6	7.2	3/6	354.9	76.9	67.6	9.8
Rb34	28.27697	86.72598	250–290	3/5	313.2	70.3	16.5	19.9	3/5	276.1	66.7	35.6	13.5
Rb35	28.28358	86.80595	250–290	6/7	11.4	0.7	22.2	12.1	6/7	11.2	20.7	22.2	12.1
Rb36	28.28107	86.80388	250–280	5/7	2.5	25.0	33.5	10.8	5/7	342.2	44.2	57.8	8.2
Rb37	28.28251	86.81231	270–290	4/7	353.0	–10.7	13.6	19.0	4/7	No structural data			
		Mean	250–280	5	359.7	29.3	4.7	39.5	4	346.4	56.9	6.2	40.2
			4 (–Rb 34)		3.9	17.8	6.9	37.6	3 (–Rb 34)	358.2	47.9	7.3	49.3
<i>Reverse 2</i>													
Rb33	28.27881	86.81017	150–250	3/6	202.2	–50.8	18.3	18.9	3/5	200.7	–71.3	17.2	19.5
Rb34	28.27697	86.72598	150–250	3/5	184.8	–41.3	20.6	17.8	6/7	168.3	–55.3	20.6	17.8
Rb35	28.28358	86.80595	150–250	2/7	190.7	–54.3	47.1	14.4	5/7	185.7	–74.2	57.8	8.2
Rb36	28.28107	86.80388	150–250	5/7	179.7	–47.5	24.4	11.6	4/7	130.7	–52.8	18.3	13.4
Rb37	28.28251	86.81231	200–270	5/7	200.5	–45.9	20.4	13.9	4	No structural data			
		Mean	150–250	5	191.4	–48.3	97.6	7.8	4	164.1	–65.8	22.5	19.8

25 Ma, the age of the main motion along the STDS (ages from shear zone) ranges from 19 to 13 Ma (see synthesis of available geochronological data and discussion in Kali et al., 2010). According to these data a remanence acquisition age younger than 20 Ma is probable for sites collected further away from the STDS shear influence and younger than 13 Ma for sites postdating deformation associated to the STDS. This possible range for the remanence age acquisition is sufficient for our purpose as the expected direction did not vary more than 5° since 20 Ma (see Table 4).

5.2. Rotations of the remanence

The influence of anisotropy on remanence directions is a critical point for the interpretation of paleomagnetic results in deformed rocks (Borradaile, 1993; Borradaile and Hamilton, 2009). Most of the examples have been observed in high grade metamorphic rocks (see Raposo et al., 2003) or in red slaty shales (Cogné and Perroud, 1985). No correlation between AMS axis and ChRM has been observed in the studied low grade metasediments. In most of the cases, AMS foliation fits with the main cleavage observed in the field while lineation corresponds to the intersection between bedding and major cleavage. When present, the cleavage is oriented in different directions according to the main folding phase. In most of the sites, pyrrhotite remanences post-date small scale deformations and therefore in averaging on site means or on regional means, we also average possible anisotropy effects. Using AARM to test the effect of anisotropy on the magnetization direction is difficult as pyrrhotite is very difficult to demagnetize using AF. El Bay et al. (2011) have imparted ARMs to highly deformed pyrrhotite rocks (gneiss) and compared the resulting direction with the

DC field used for producing the ARM. Even in these highly dominated crystalline rocks no significant influence of pyrrhotite anisotropy on remanence directions could be observed. Therefore, we assume that in sedimentary rocks, where bedding is clearly visible, the influence of pyrrhotite anisotropy on remanence direction can be neglected.

Comparing the regional mean direction from Dinggye area ($D/I = 351.7^\circ/25.1^\circ$, $k = 13.1$, $\alpha_{95} = 9.4^\circ$, $N = 20$) to the direction expected from the apparent polar wander path (APWP) of stable India at 15 Ma (calculated from Besse and Courtillot, 2002; Table 4) suggests that significant counterclockwise rotation, of about $11.9 \pm 8.7^\circ$, around a vertical axis has occurred (Fig. 11 and Table 5). For Kharta area ($D/I = 20.6^\circ/37.5^\circ$, $k = 51.9$, $\alpha_{95} = 6.9^\circ$, $N = 8$), the same comparison leads to a clockwise rotation of about $17.0 \pm 7.5^\circ$ for an age of 15 Ma. The results of the R2 component ($D/I = 191.4^\circ/-48.3^\circ$, $k = 97.6$, $\alpha_{95} = 7.8^\circ$, $N = 5$) from Rongbuk area (i.e., acquired after the deformation associated to the motion along the STDS) do not indicate a significant rotation ($7.8 \pm 9.7^\circ$ clockwise since 15 Ma).

Paleomagnetic data from the HHC south of the Everest massif (Rochette et al., 1994; El Bay et al., 2011) are also showing an apparent clockwise rotation ($14.8 \pm 7.7^\circ$ and $38.7 \pm 15.9^\circ$, respectively). As already suggested by El Bay et al. (2011) for results from Imja Khola, the departure from the expected direction can be interpreted as tilting around a horizontal axis producing a small circle distribution of remanence directions (Fig. 11). The direction of tilting is eastward for Dinggye while it is westward for Everest, Imja Khola and Kharta areas. The directions and values of tilting are given in Table 5. Using paleomagnetic results from Dinggye, Kharta, Imja Khola and Everest, a best fit small circle was calculated (direc-

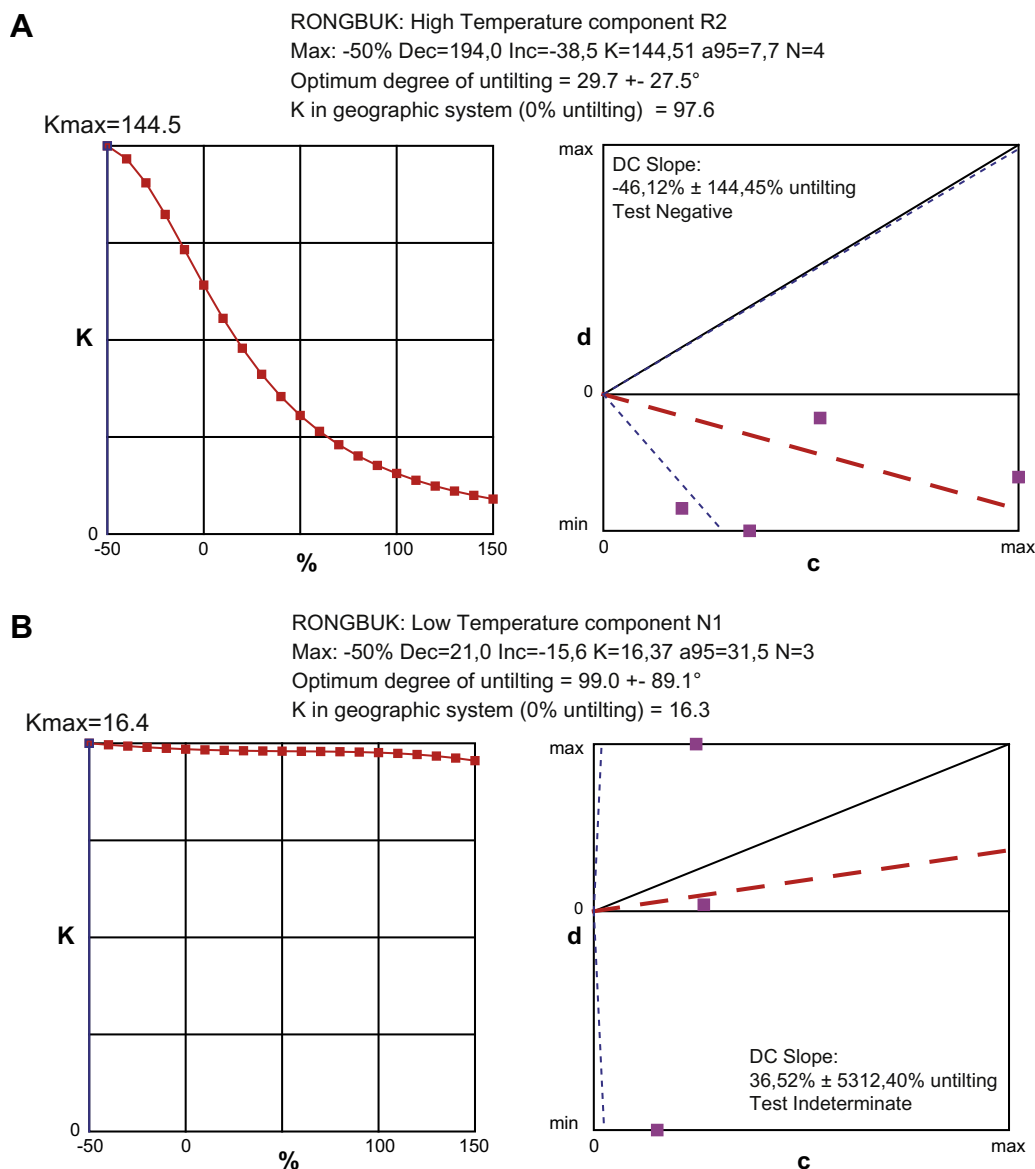


Fig. 9. Fold tests for A: the high temperature (N1) and B: the low temperature (R2) components from Rongbuk area. See Fig. 6 for explanations.

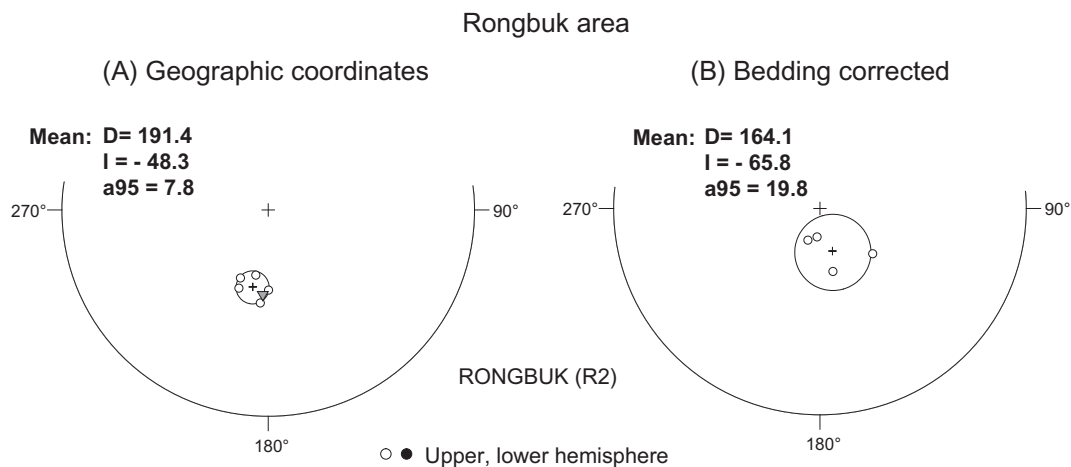


Fig. 10. Stereographic projection of the pyrrhotite site mean directions for R2 component from Rongbuk area. The overall mean direction obtained by Fisher statistics is indicated. Open (solid) circles are projected in the upper (lower) hemisphere. (A) In situ (geographic coordinates), (B) Bedding corrected. The present-day dipole field direction is indicated by a triangle in (A).

Table 4

Expected directions versus age, calculated from the master APWP of Besse and Courtillot (2002) for a location at latitude = 28.2°N and longitude = 87.8°E. Dec.: declination; Inc.: inclination; α_{95} : 95% confidence angle; dDec. (dInc.): declination (inclination) uncertainty, calculated after Demarest (1983).

Age in Ma	Expected direction Master APWP BC 2002				
	Dec.	Inc.	α_{95}	dDec.	dInc.
0	3.2	45.8	2.4	3.4	3.7
5	3.4	45.7	2.0	2.9	3.2
10	2.8	42.7	2.5	3.4	4.1
15	3.3	41.8	2.6	3.5	4.3
20	5.2	41.0	3.7	4.9	6.1
25	0.5	35.3	4.9	6.0	8.5
30	1.1	25.0	5.1	8.7	8.7
35	0.4	25.3	4.2	4.6	7.8
40	0.9	25.0	6.7	7.4	12.5
45	3.3	17.7	5.3	5.6	10.2
50	4.1	12.3	4.4	4.5	8.7
55	4.8	-1.5	4.8	4.8	9.6
60	6.2	-20.4	4.4	4.7	8.4

Site location: Lat = 28.2°N/Long = 87.8°E.

tion: 19.7°, opening angle: 40.4°). The expected direction ($D/I = 3.3^\circ/41.8^\circ$) at 15 Ma is close to the calculated small circle. Therefore, the paleomagnetic results can be explained by tilting around only one axis i.e. along the calculated best fit small circle, from the expected direction to the observed one (Fig. 11 and Table 5). The axis of the small circle has a very similar direction as the ADM and also as the Xainza–Dinggye normal fault (XDNF) which is one of the numerous N–S structures that accommodate the E–W extension of the Tibetan Plateau. In the study area, the XDNF is striking N15–N35 with an eastward dipping angle of about 40–50° (Zhang and Guo, 2007).

A possible alternative model to explain the observed data resides in combining vertical-axis rotation and tilting around horizontal axis. A vertical-axis clockwise rotation (16.4°) and

subsequent tilting (around a horizontal axis) is possible. The vertical axis rotation is given by the difference between the axis of the small circle fitting with the paleomagnetic directions (19.7°) and the expected direction (3.3° at 15 Ma). The clockwise rotation may be associated to a large-scale dextral shearing linked to the eastward extrusion of the Tibetan Plateau (Pêcher, 1991; Schill et al., 2004). However, our results from Rongbuk and earlier results from Tingri (Appel et al., 1998) do not support a uniform significant clockwise rotation. Therefore, the first scenario with only one rotation around a horizontal axis is preferred.

The small circle distribution of the regional mean directions can be interpreted as the result of a crustal doming structure such as the one suggested by El Bay et al. (2011) for the interpretation of Imja Khola data. In the present contribution, the Rongbuk, Imja Khola, Kharta and Dinggye data are interpreted in the same model (Fig. 12). This interpretation is consistent with regional geological structures such as the Arun antiform with a ~N–S axis (Bordet, 1961) and the ADM horst (Kali et al., 2010). Tilting angles shown in Fig. 12 represent the angular differences of the area mean directions and the expected directions along the best fit small circle (more precisely: between their projections on the small circles). The Imja Khola data have been projected according to the mean direction of the Sangkar–Kharta fault zone bounding the ADM to the west. The tiltings recorded by paleomagnetic data are due to several processes such as normal faults or the uplift of the Ama Drime Massif in an extensional tectonic regime as it is well described in literature (see Jessup et al. 2008; Cottle et al., 2009; Langille et al., 2010). Only tilting angles from Dinggye and Kharta are used in order to quantify the maximum uplift (avoiding other possible parameters), because they are the closest available data. Using a very simple approach, tilting angle is associated to the distance from central part of the ADM, and it allows the calculation of 15.5 ± 9.4 km of uplift since remanence acquisition (end of motion along the STDS). If an age of 13 Ma is assumed, a constant mean exhumation rate can be estimated at $ca\ 1.2 \pm 0.7$ mm/yr. According

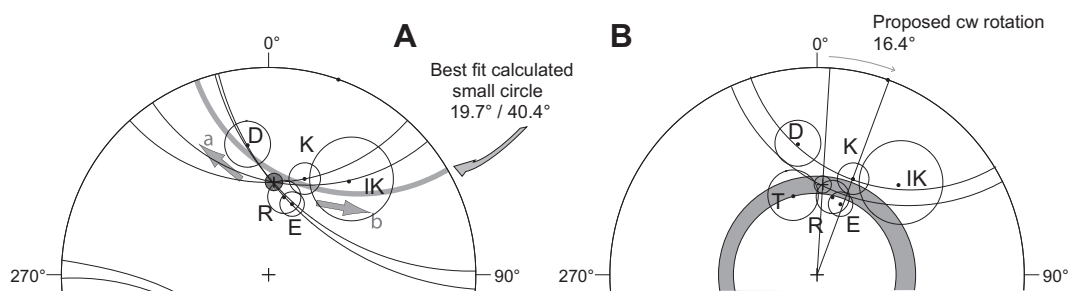


Fig. 11. Stereographic projection of regional mean directions. The expected direction ($D = 3.3^\circ$, $I = 41.8^\circ$) for 15 Ma is indicated. A: Illustration of the horizontal axis tilting model. Arrow a (b) indicates eastward (westward) tilting. The small circles are indicated. The regional best fitting small circle is illustrated. B: A proposed clockwise rotation model of ~16.4° is illustrated. Everest and Rongbuk directions are plotted as normal component. D: Dinggye, K: Kharta, R: Rongbuk, E: Everest (Rochette et al., 1994), T: Tingri (Appel et al., 1998), IK: Imja Khola (El Bay et al., 2011), +: expected direction at 15 Ma.

Table 5

Regional mean paleomagnetic directions (Dec: declination; Inc: inclination; α_{95} : 95% confidence angle) from this study and (1): El Bay et al. (2011); (2): Rochette et al. (1994); (3): Appel et al. (1998). Rotation around vertical axis (R) calculated for a remanence age of 15 Ma, uncertainty on the rotation (dR) was calculated after Demarest (1983). Tilting direction and angle according to one rotation model are indicated.

	Dec.	Inc.	α_{95}	R	dR	Tilt direction	Tilting angle
Dinggye	351.7	25.1	9.4	-11.9	8.7	127	28 ± 12
Kharta	20.6	37.5	6.9	17.0	7.5	270	20 ± 9.5
Rongbuk	191.4	-48.3	7.8	7.8	9.7	308	10 ± 10.4
Imja Khola (1)	42.3	29.4	17.2	38.7	15.9	278	52 ± 19.8
Everest (2)	198.4	-50.6	5.7	14.8	7.7	310	16 ± 8.3
Tingri (3)	343.2	46.8	12	-20.4	14.3	*	*

Tilting angle along small circle ($D = 19.7$ opening = 40.8).

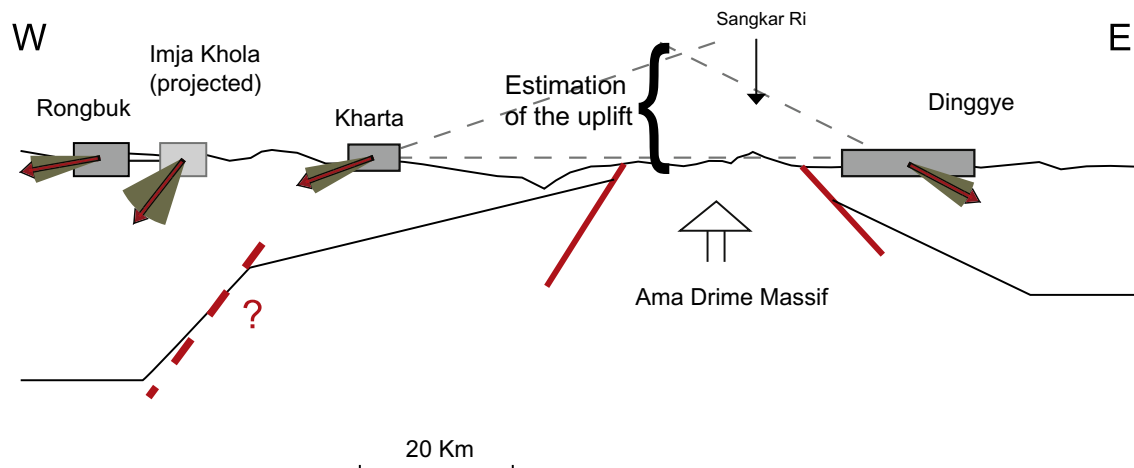


Fig. 12. Model of crustal doming explaining the observed deviation of the paleomagnetic directions from the expected Earth magnetic dipole field direction at the time of remanence acquisition (~15 Ma). Tilting angles are indicated with uncertainty. Notice that tiltings are not due to motion along normal faults but may be related to the uplift of the Ama Drime Massif.

to Spicer et al. (2003), the elevation of the southern Tibetan plateau probably has remained unchanged for the past 15 Myr; consequently the uplift estimated above is restricted to the ADM range.

6. Conclusion

In this study, we present new paleomagnetic data from low grade metamorphic Tethyan Himalaya sediments around the Ama Drime Massif in S-Tibet. The remanences are residing in pyrrhotite and were likely acquired during exhumation of the ADM. The existence of antipodal pTRMs demonstrates that the ChRM is of thermoremanent origin and was acquired during cooling of the Tethyan metasediments while penetrative deformation was still going on in Rongbuk area until cooling through ca 250 °C, whereas it was already completed in Dinggye area. The departures from the expected field direction during the age of remanence acquisition can be interpreted as tilting around a horizontal axis striking N20° and can be estimated to be younger than 13–12 Ma. These tiltings are associated to the ADM exhumation initiated since 33 Ma.

Acknowledgments

We thank reviews for helpful and constructive comments. The German Research Council (DFG) funded this study within Project AP 34/24-1,2; part of the work was done within the DFG Priority Programme 1372 'Tibetan Plateau: Formation, Climate, Ecosystems (TiP)'. We thank H. Leloup for discussions and advices.

References

- Antolín, B., Appel, E., Gloaguen, R., Dunkl, I., Ding, L., Montomoli, C., Liebke, U., Xu, Q., 2010. Paleomagnetic evidence for clockwise rotation and tilting in the eastern Tethyan Himalaya (SE Tibet): implications for the miocene tectonic evolution of the NE Himalaya. *Tectonophysics* 493, 172–186.
- Antolín, B., Appel, A., Montomoli, C., Dunkl, I., Ding, L., Gloaguen, R., El Bay, R., 2011. Kinematic evolution of the eastern Tethyan Himalaya: constraints from magnetic fabric and structural properties of the Triassic flysch in SE Tibet. In: Poblet, J., Lisle R., (Eds.), *Kinematic Evolution and Structural Styles of Fold-and-Thrust Belts*. vol. 349. Geological Society of London Special Publications, pp. 99–121.
- Appel, E., Müller, R., Widder, R.W., 1991. Paleomagnetic results from the Tibetan sedimentary series of the manange area (north central Nepal). *Geophys. J. Int.* 104, 255–266.
- Appel, E., Patzelt, A., Chouker, C., 1995. Secondary palaeoremanence of Tethyan sediments from the Zaskar Range (NW Himalaya). *Geophys. J. Int.* 122, 227–242.

- Appel, E., Li, H., Patzelt, A., Wang, J., 1998. Palaeomagnetic results from late cretaceous and early tertiary limestones from the Tingri area in southern Tibet. *J. Nepal Geol. Soc.* 18, 113–124.
- Armijo, R., Tapponier, P., Mercier, J.L., Tonglin, H., 1986. Quaternary extension of the Tibetan Plateau: field observations and tectonic implications. *J. Geophys. Res.* 91 (B14), 13803–13872.
- Bassoulet, J.P., Boulin, J., Colchen, M., Marcoux, J., Mascle, G., Montenat, C., 1980. Evolution des domaines Téthysiens au pourtour du Bouclier Indien du Carbonifère au Crétacé. *Géologie des Chaînes Alpines issues de la Téthys, Colloque C5*. In: 26th International Geological Congress, Mém. BRGM, Paris, vol. 115, pp. 180–198.
- Besnus, M.J., 1966. Propriétés magnétiques de la pyrrhotite naturelle. PhD Thesis University of Strasbourg.
- Besse, J., Courtillot, V., 2002. Apparent and true polar wander and the geometry of the geomagnetic field over the last 200 Myr. *J. Geophys. Res.* 107, 2300. <http://dx.doi.org/10.1029/2000JB000050>.
- Bordet, P., 1961. Recherches Géologiques dans l'Himalaya du Népal, Région du Makalu. *Cent. Natl. de la Rech. Sci., Paris*, pp. 275.
- Borradaile, G.J., 1993. Strain and remanence. *J. Struct. Geol.* 15, 383–390.
- Borradaile, G.J., Hamilton, T.D., 2009. Re-computing palaeopoles for the effects of tectonic finite strain. *Tectonophysics* 467, 131–144.
- Brookfield, M.E., 1993. The Himalayan passive margin from Precambrian to Cretaceous time. *Sediment. Geol.* 84, 1–35.
- Carpenter, R.H., 1974. Pyrrhotite isograd in the SE Tennessee and SW North Carolina. *Geol. Soc. Amer. Bull.* 85, 451–456.
- Carosi, R., Montomoli, C., Visonà, D., 2002. Is there any detachment in the Lower Dolpo (western Nepal)? *C. R. Geoscience* 334, 933–940.
- Carosi, R., Montomoli, C., Visonà, D., 2007. A structural transect in the Lower Dolpo: Insights on the tectonic evolution of Western Nepal. *J. Asian Earth Sci.* 29, 407–423.
- Cogné, J.P., Perroud, H., 1985. Strain removal applied to paleomagnetic directions in an orogenic belt: the Permian red slates of the Alpes Maritimes, France. *Earth Planet. Sci. Lett.* 72, 125–140.
- Cottle, J.M., Jessup, M.J., Newell, D.L., Horstwood, M.S.A., Noble, S.R., Parrish, R.R., Waters, D.J., Searle, M.P., 2009. Geochronology of granulitized eclogite from the Ama Drime Massif: implications for the tectonic evolution of the South Tibetan Himalaya. *Tectonics* 28, TC1002. <http://dx.doi.org/10.1029/2008TC002256>.
- Crouzet, C., Ménard, G., Rochette, P., 1996. Post middle Miocene rotations recorded in the Bourg d'Oisans area (Western Alps) by paleomagnetism. *Tectonophysics* 263, 137–148.
- Crouzet, C., Rochette, P., Ménard, G., Prévot, M., 1997. Acquisition d'aimantations thermorémanentes partielles successives portées par la pyrrhotite monodomaine lors du refroidissement de la zone dauphinoise interne (Alpes occidentales, France). *Compte Rendu Acad. Sci. Paris II* 325, 643–649.
- Crouzet, C., Rochette, P., Ménard, G., 2001a. Experimental evaluation of thermal recording of polarity reversals during metasediments uplift. *Geophys. J. Int.* 145, 771–785.
- Crouzet, C., Stang, H., Appel, E., Schill, E., Gautam, P., 2001b. Detailed analysis of successive pTRMs carried by pyrrhotite in Himalayan metacarbonates: an example from Hidden Valley Central Nepal. *Geophys. J. Int.* 146, 607–618.
- Crouzet, C., Gautam, P., Schill, E., Appel, E., 2003. Multicomponent magnetization in Western Dolpo (Tethyan Himalaya, Nepal): implications for tectonic motions. *Tectonophysics* 377, 179–196.
- Crouzet, C., Dunkl, I., Paudel, L., Arkai, P., Rainer, T.M., Balogh, K., Appel, E., 2007. Temperature and age constraints on the metamorphism of the Tethyan Himalaya in Central Nepal: a multidisciplinary approach. *J. Asian Earth Sci.* 30, 113–130.

- Demarest, H., 1983. Error analysis for the determination of tectonic rotation from paleomagnetic data. *J. Geophys. Res.* 88, 4321–4328.
- Dunkl, I., Antolin, B., Wemmer, K., Rantitsch, G., Kienast, M., Montomoli, C., Ding, L., Carosi, R., Appel, E., El Bay, R., Xu, Q., Von Eynatten, H., 2011. Metamorphic evolution of the Tethyan Himalayan flysch in SE Tibet. In: Gloaguen, R., Ratschbacher, L. (Eds.), *Growth and Collapse of the Tibetan Plateau*. Geological Society, London, Special Publications vol. 353, pp. 45–69.
- El Bay, R., Appel, E., Paudel, L., Neumann, U., Setzer, F., 2011. Palaeomagnetic remanences in high grade metamorphic rocks of the Everest region: indication for late Miocene crustal doming. *Geophys. J. Int.* <http://dx.doi.org/10.1111/j.1365-246X.2011.05078.x>.
- Enkin, R.J., 2003. The direction-correction tilt test: an all-purpose tilt/fold test for paleomagnetic studies. *Earth Planet. Sci. Lett.* 212, 151–166.
- Enkin, R.J., 2004. Paleomagnetism data analysis: version 4.2. *Geol. Surv. Can., Sidney, BC*. <<http://www.pgc.nrcan.gc.ca/tectonic/enkin.htm>>.
- Fuchs, G., 1967. Zum Bau des Himalaya. *Osterreichische akademie der wissenschaften, mathematisch-naturwissenschaftliche klasse. Denkschriften* 113, 1–211.
- Garzanti, E., 1999. Stratigraphy and sedimentary history of the Nepal Tethyan Himalaya passive margin. *J. Asian Earth Sci.* 17, 805–827.
- Gillett, S.L., 2003. Paleomagnetism of the notch peak metamorphic aureole, revisited: pyrrhotite from magnetite + pyrite under submetamorphic conditions. *J. Geophys. Res.* 108 (B9), 2446. <http://dx.doi.org/10.1029/2002JB002386>.
- Gloaguen, R., Ratschbacher, L., 2011. Growth and collapse of the Tibetan Plateau: introduction. *Geological Society London, Special Publications vol. 353*, pp. 1–8. doi: 10.1144/SP353.1.
- Godin, L., Gleeson, T.P., Searle, M.P., Ulrich, T.D., Parrish, R.R., 2006. Locking of southward extrusion in favour of rapid crustal-scale buckling of the Greater Himalayan sequence, Nar valley, central Nepal. In: Law, R.D., Searle, M.P., Godin, L. (Eds.), *Channel Flow, Ductile Extrusion and Exhumation in Continental Collision Zones*. Geological Society, London, Special Publications, vol. 268, pp. 269–292.
- Godin, L., 2003. Structural evolution of the Tethyan sedimentary sequence in the Annapurna area, central Nepal Himalaya. *J. Asian Earth Sci.* 22, 307–328. [http://dx.doi.org/10.1016/S1367-9120\(03\)00066](http://dx.doi.org/10.1016/S1367-9120(03)00066).
- Groppo, C., Lombardo, B., Rolfo, F., Pertusati, P., 2007. Clockwise exhumation path of granulitized eclogites from the Ama Drime range (Eastern Himalayas). *J. Metamorph. Geol.* 25, 51–75. <http://dx.doi.org/10.1111/j.1525-1314.2006.00678.x>.
- Hodges, K.V., 2000. Tectonics of the Himalaya and southern Tibet from two perspectives. *Geol. Soc. Am. Bull.* 112, 324–350.
- Jessup, M.J., Cottle, J.M., Searle, M.P., Law, R.D., Newell, D.L., Tracy, R.J., Waters, D.J., 2008. P–T–D paths of Everest Series schist, Nepal. *J. Metamorph. Geol.* 26, 717–739. <http://dx.doi.org/10.1111/j.1525-1314.2008.00784.x>.
- Kali, E., Leloup, P.H., Arnaud, N., Mahéo, G., Liu, D., Boutonnet, E., Van der Woerd, J., Xiaohan, L., Jing Liu-Zeng, Li, H., 2010. Exhumation history of the deepest central Himalayan rocks (Ama Drime range): key P–T–D–t constraints on orogenic models. *Tectonics* 292 (1–2), 1–16.
- Kellett, D.A., Godin, L., 2009. Pre-Miocene deformation of the Himalayan superstructure, Hidden valley, central Nepal. *J. Geol. Soc.* 166 (2), 261–275. <http://dx.doi.org/10.1144/0016-76492008-097>.
- Kim, W., Doh, S.-J., Yu, Y., Lee, J.J., Suk, D., 2009. Hydrothermal fluid-controlled remagnetization of sedimentary rocks in Korea: tectonic importance of pervasive Tertiary remagnetization. *Tectonophysics* 474 (3–4), 684–695.
- Kirschvink, J.L., 1980. The least-squares line and plane and the analysis of palaeomagnetic data. *Geophys. J. R. Astr. Soc.* 62, 699–718.
- Klootwijk, C.T., Bingham, D., 1980. The extent of greater India, III. Palaeomagnetic data from the Tibetan sedimentary series, Thakkhola region, Nepal Himalaya. *Earth Planet. Sci. Lett.* 51, 381–405.
- Langille, J.M., Jessup, M.J., Cottle, J.M., Newell, D., Seward, G., 2010. Kinematic evolution of the Ama Drime detachment: Insights into orogen-parallel extension and exhumation of the Ama Drime Massif, Tibet–Nepal. *J. Struct. Geol.* 32, 900–919.
- Larson, K.P., Godin, L., Davis, W.J., Davis, D.W., 2010. Out-of-sequence deformation and expansion of the Himalayan orogenic wedge: insight from the Chango culmination, south-central Tibet. *Tectonics* 29 (TC4013), 30. <http://dx.doi.org/10.1029/2008TC002393>.
- Leloup, P.H., Kali, E., Arnaud, N., Mahéo, G., Boutonnet, E., Liu, X., Liu, D., Li, H., Liu-Zeng, J., 2009. Miocene (~12 Ma) transition from E–W to N–S syn-convergence normal faulting in the central Himalayas (Ama Drime range). *Geophys. Res. Abstr.* pp. 11, EGU2009-9690-2001.
- Leloup, P.H., Maheo, G., Arnaud, N., Kali, E., Boutonnet, E., Liu, D., Liu, X., Li, H., 2010. The South Tibet detachment shear zone in the Dinggye area: time constraints on extrusion models of the Himalayas. *Earth Planet. Sci. Lett.* 292, 1–16. <http://dx.doi.org/10.1016/j.epsl.2009.12.035>.
- Liu, Y., Siebel, W., Massonne, H.J., Xiao, X.C., 2007. Geochronological and petrological constraints for tectonic evolution of the central Greater Himalayan Sequence in the Kharta area, southern Tibet. *J. Geol.* 115, 215–230. <http://dx.doi.org/10.1086/510806>.
- Lombardo, B., Rolfo, F., 2000. Two contrasting eclogite types in the Himalayas: implications for the Himalayan orogeny. *J. Geodyn.* 30, 37–60. [http://dx.doi.org/10.1016/S0264-3707\(99\)00026-5](http://dx.doi.org/10.1016/S0264-3707(99)00026-5).
- Ménard, G., Rochette, P., 1992. Utilisation de réaimentation postmétamorphiques pour une étude de l'évolution tectonique et thermique tardive dans les Alpes occidentales (France). *Bull. Soc. Géol. France* 163 (4), 381–392.
- Montomoli, C., Appel, E., Antolin, B., Dunkl, I., El Bay, R., Lin, D., Gloaguen, R., 2008. Polyphase deformation history of the “Tibetan Sedimentary Sequence” in the Himalaya chain (South-East Tibet). 23th Himalaya–Karakoram–Tibet workshop extended abstracts. *Himalayan J. Sci.* 5, 91.
- Montomoli, C., Carosi, R., Carulli, A., Appel, E., Ding, L., Dunkl, I., El Bay, R., Leiss, B., 2009. Deformation, kinematic and metamorphism of the South Tibetan Detachment System in the Dinggye section (Southern Tibet). 24th Himalayan – Karakorum–Tibet workshop, Beijing, abstract volume.
- McFadden, P.L., McElhinny, M.W., 1988. The combined analysis of remagnetisation circles and direct observations in palaeomagnetism. *Earth Planet. Sci. Lett.* 87, 161–172.
- Patzelt, A., 1996. Palaeo- and rockmagnetism of Cretaceous to Tertiary sediments from the Tethyan Himalaya: evidence for crustal shortening and deformation of the northern Indian margin due to the collision with Eurasia. *Tübinger Geowissenschaftliche Arbeiten, Reihe A* 25, 83p.
- Pêcher, A., 1991. The contact between the Higher Himalaya crystallines and the Tibetan sedimentary series: miocene large scale dextral shearing. *Tectonics* 10 (3), 587–598.
- Raposo, M.I.B., D'Agrella-Filho, M.S., Siqueira, R., 2003. The effect of magnetic anisotropy on paleomagnetic directions in high-grade metamorphic rocks from the Juiz de Fora Complex, SE Brazil. *Earth Planet. Sci. Lett.* 209, 131–147.
- Ratschbacher, L., Frisch, W., Liu, G., Cheng, C.C., 1994. Distributed deformation in Southern and Western Tibet as result of the India–Asia collision. *J. Geophys. Res.* 99 (B10), 19917–19945.
- Rochette, P., 1987. Metamorphic control of the magnetic mineralogy of black shales in the Swiss Alps, toward the use of «magnetic isograds». *Earth Planet. Sci. Lett.* 84, 446–456.
- Rochette, P., Fillion, G., Dekkers, M.J., 2011. Interpretation of low-temperature data. Part 4: The low-temperature magnetic transition of monoclinic pyrrhotite. *IRM Quarterly* 21, 1.
- Rochette, P., Fillion, G., Mattéi, J.-L., Dekkers, M.J., 1990. Magnetic transition at 30–40 Kelvin in pyrrhotite: insight into a widespread occurrence of this mineral in rocks. *Earth Planet. Sci. Lett.* 98, 319–328.
- Rochette, P., Scailliet, B., Guillot, S., LeFort, P., Pêcher, A., 1994. Magnetic properties of the High Himalayan leucogranites: structural implications. *Earth Planet. Sci. Lett.* 126, 214–234.
- Schill, E., Appel, E., Zeh, O., Singh, V.K., Gautam, P., 2001. Coupling of late-orogenic tectonics and secondary pyrrhotite remanences: towards a separation of different rotation processes and quantification of rotational underthrusting in the western Himalayas (N-India). *Tectonophysics* 337, 1–21.
- Schill, E., Appel, E., Gautam, P., Dietrich, P., 2002. Thermo-tectonic history of the Tethyan Himalayas deduced from the palaeomagnetic record of metacarbonates from Shiari Khola (Central Nepal). *J. Asian Earth Sci.* 20, 203–210.
- Schill, E., Appel, E., Godin, L., Crouzet, C., Gautam, P., Regmi, K.R., 2003. Record of deformation by secondary magnetic remanences and magnetic anisotropy in the Nar/Phu valley (Central Himalaya). *Tectonophysics* 377, 197–209.
- Schill, E., Appel, E., Crouzet, C., Gautam, P., Wehland, F., Staiger, M., 2004. Oroclinal bending and regional significant clockwise rotations of the Himalayan arc – constraints from secondary pyrrhotite remanences. In: Sussman, A.J., Weil, A.B., *Orogenic Curvature: Integrating Paleomagnetic and Structural Analysis*. *Geol. Soc. Am. Spec. Paper*, vol. 383, pp. 73–85.
- Spicer, R.A., Harris, N.B.W., Widdowson, M., Herman, A.B., Guo, S., Valdes, P.J., Wolfe, J.A., Kelley, S.P., 2003. Constant elevation of southern Tibet over the past 15 million years. *Nature*, 622–624. <http://dx.doi.org/10.1038/nature01356>.
- Vannay, J.C., Hodges, K.V., 1996. Tectonometamorphic evolution of the Himalayan metamorphic core between the Annapurna and Dhaulagiri, central Nepal. *J. Metamorph. Geol.* 14, 635–656.
- Watson, G.S., Enkin, R.J., 1993. The fold test in paleomagnetism as a parameter estimation problem. *Geophys. Res. Lett.* 20, 2135–2137.
- Wehland, F., Eibl, O., Braun, S., Alt-Epping, U., Appel, E., 2005. Pyrrhotite pTRM acquisition in metamorphic limestones in the light of microscopic observations. *Phys. Earth Planet. Inter.* 151, 107–114.
- Zhang, J., Guo, L., 2007. Structure and geochronology of the southern Xainza–Dinggye rift and its relationship to the south Tibetan detachment system. *J. Asian Earth Sci.* 29, 722–736.